• **Title:** *Discrete Element Modeling of Stick-Slip Instability and Induced Microseismicity[1]*

• **Author names and affiliations:**

1- **Cyrus Khazaei, PhD student (Corresponding Author) [1]**
2- **Jim Hazzard, PhD, PEng [2]**
3- **Rick Chalaturnyk, PhD, PEng [1]**

[1] NREF/CNRL Markin Bldg

Department of Civil and Environmental Engineering

University of Alberta

Edmonton, Alberta, Canada T6G 2W2

Em: khazaei@ualberta.ca

Em: rjchalaturnyk@ualberta.ca

[2] Itasca Consulting Group Inc.

Toronto, Ontario, Canada M5C 1H6

Em: jhazzard@itascacg.com

---

i

Contents

Abstract

Using Particle Flow Code (PFC3D), a discrete element model is presented in this paper that allows direct modeling of stick-slip behavior in pre-existing weak planes such as joints, beddings and faults. The model is used to simulate a biaxial sliding experiment from literature on a saw-cut specimen of Sierra granite with a single fault. The fault is represented by Smooth Joint Contact Model. Also, an algorithm is developed to record the stick-slip induced microseismic events along the fault. Once the results compared well with laboratory data, a parametric study has been conducted to investigate the evolution of model's behavior due to varying factors such as resolution of the model, particles' elasticity, fault's coefficient of friction, fault's stiffness and normal stress.

The results show a decrease in shear strength of the fault in the models with smaller particles, smaller coefficient of friction of the fault, harder surrounding of the fault, softer faults and smaller normal stress on the fault. Also, a higher rate of displacements was observed for conditions resulting in smaller shear strength. An increase in b-values was observed by increasing the resolution or decreasing the normal stress on the fault while b-values were not sensitive to changes in elasticity of the fault or its surrounding. A larger number of recorded events were observed for the models with finer particles, smaller fault's coefficient of friction, harder fault's surrounding, harder fault and smaller normal stress on the fault. The results suggest that it is possible for the two ends of a fault to be still while there are patches along the fault undergoing stick-slips. Such local stick-slips seem to provide a softer surrounding for their neighbor patches facilitating their subsequent stick-slips.

Keywords: Stick-slip, Particle Flow Code (PFC), Microseismic, Fault Instability

1. Introduction

It is believed that the mechanism of fault's instability involves multiple local on and off slips of patches referred to as "stick-slip" along the fault (Brace & Byerlee, 1966). Such small stick-slips may be recorded as "foreshocks" leading to "main shocks" and followed by "aftershocks" each releasing different levels of acoustic energy. Various aspects of fault's instability has been already studied by laboratory experiments (Brune et al., 1993; Byerlee & Brace, 1968; Dieterich, 1981; Julian et al., 1998; Ohnaka, 1973) as well as numerical continuum models (Dalguer & Day, 2006; Day et al., 2005; Galis et al., 2008; Xing et al., 2004) and numerical discontinuum models (Finch et al., 2003; Mora & Place, 1994; Morgan, 2004; Place et al., 2002).

Compared to continuum models, Discrete Element Method (DEM) has the capability of modeling geometrical heterogeneity by size distribution of particles as well as looking into the rupture process of rocks with more details. Using Particle Flow Code (PFC3D) v.5.0 in this research, a discrete representation of the fault is modeled and release of acoustic energy due to its stick-slip instability is studied. For this purpose, a large scale laboratory experiment conducted on granite with a single fault originally reported by Dieterich (1979) and recently repeated with microseismic recording by McLaskey & Kilgore (2013) has been numerically simulated.

Traditionally, the approach for modeling microseismicity with PFC has been to consider each bond breakage (crack) as a single AE event with further possibility of clustering the events to form more realistic magnitudes (Hazzard, 1998). This approach has been successfully used in modeling the intact rock problems where the events are believed to have a compressive

induced crack nature (Hazzard & Young, 2002, 2004; Young et al., 2005, 2001; Zhao & Young, 2011). However, in the present research, new routines have been developed for recording slip-induced microseismic events. The results have been compared with the experimental data. Then, a parametric study has been conducted to study the effect of various factors on fault's behavior.

This knowledge could also be useful for problems other than earthquake studies where there is likelihood of two planes sliding on each other such as landslides (Peng & Gomberg, 2010), basal gliding of ice glaciers (Jansen, 2006; Roux et al., 2008) and microseismic monitoring of a sedimentary rock mass in Petroleum projects (Fairhurst, 2013; Kristiansen et al., 2000).

2. Theory of Slip

The basics of how slip occurs in physics are briefly explained using Figure 1 (left). As the applied driving force to the block, f_d, is increased, the resistive frictional force (solid red line) is increased too until at point a, f_d reaches the maximum static frictional resistance, the frictional resistance drops to lower values known as kinetic friction (or as simplified by the dotted blue curve), the spring unloads following a line with the slope equal to its stiffness (dashed green line), K, and the block starts to move.

The spring's unloading continues even after the applied force equals to kinetic friction at point c, meaning deceleration of the block until the final stop at point e where the excess energy is dissipated (Δabc equals Δcde) (Scholz, 2002). In reality, once the motion eventually stops (point e), there has to be a "healing" mechanism for friction to regain its static value so that further slips could happen.
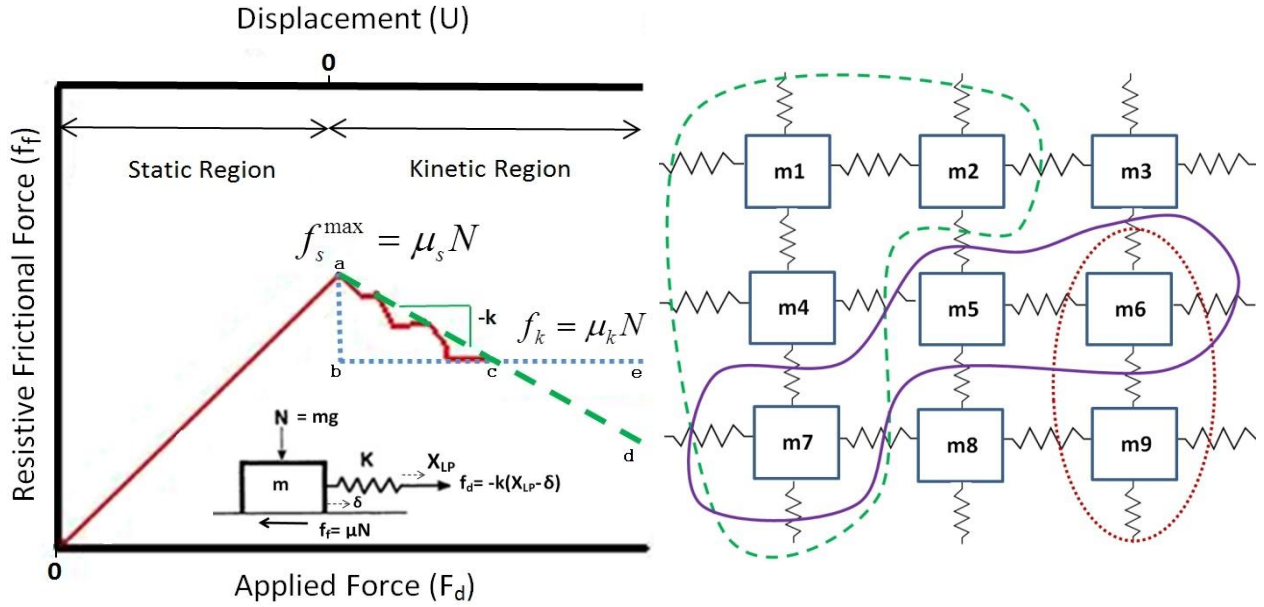
Figure 1: (Left) Solid red line is variations of the resistive frictional force. The simplified change in friction is shown in dotted blue. The dashed green line shows variations of the driving force once the block starts to move until it stops. (Right) Horizontal section of a more realistic model for the fault. The masses, stiffness of springs and normal stress on each block are not necessarily equal due to heterogeneity. Three arbitrary patches are shown with dotted red, solid purple and dashed green. The red and green patches can slide simultaneously.

This process of multiple slips and stops is called "stick-slip" and is believed to be the mechanism of earthquakes (Brace & Byerlee, 1970). Rabinowicz (1951, 1958) first suggested that if two surfaces are in contact in a stationary condition under load for time t, the coefficient of static friction increases approximately as $logt$. He also proposed that a minimum displacement of Dc, "critical slip distance", is required for transition from static friction state to kinetic friction state. With regard to Figure 1 (left), the condition required for the onset of instability can be mathematically expressed by Eq. (1):

$$\left| \frac{\partial f_f}{\partial u} \right| = \frac{(\mu_s - \mu_k)N}{D_c} > K \tag{1}$$

where $\left| \partial f_f \middle/ \partial u \right|$ is variations of resistive frictional force, f_f, for increments of displacement, u.

The parameters μ_s and μ_k are static and kinetic coefficients of friction, respectively, N is the normal stress on the block, D_c is critical slip distance and K is the stiffness of spring.

The physical implication of the stiffness of spring in this model, K, can be thought of as the elastic conditions of the vicinity of a fault in nature or the stiffness of the loading machine in the laboratory. From Eq. (1), it is obvious that instability depends on the normal stress, elastic properties of the medium surrounding the fault and roughness of the fault. The major microseismic events in the field are believed to be the result of stress drop followed by slip on fractures and consequently release of energy (Damjanac et al., 2010). However, if the stress drop is not large enough to impose excess energy to the system (i.e. after point "*a*" in Figure 1 (left), the drop in resistive frictional force (solid red line) is such that it is placed above the unloading line (dashed green line), the slip would be aseismic. Therefore, in reality not every slip is the source of instability and considered as seismic.

The assumption behind the model explained by Figure 1 (left) is that the block can be regarded as a single mass point. Persson & Tosatti (1999) suggest that for this assumption to be valid the dimension of block, L_B, has to be smaller than a characteristic "elastic coherence length", ξ, otherwise, the block has to be discretized to smaller cells with the size, ξ, connected to each other by elastic springs. Therefore, it is necessary to take into account heterogeneity and nonuniform geometry of faults (Nielsen et al., 2000, 1995). A more realistic model for the fault is shown in Figure 1 (right). In this model, the mass, stiffness of springs and normal stress on

each block is different and thus different patches may form and slide at different times or simultaneously.

3. Description of the Experiment

Dieterich (1979) studied the scale dependence of fault instability process through a large scale biaxial laboratory experiment. A large specimen of Sierra white granite with 1.5x1.5x0.419 m dimensions was sawed diagonally at the quarry and roughened in the laboratory by lapping the two surfaces together with 30 grit silicon carbide abrasive to represent the fault with peak-to-trough surface roughness of 0.08 mm (Dieterich, 1981). He concluded that a minimum fault length was required so that confined shear instability could occur along a preexisting fault. Although strain gauges and velocity transducers were mounted on the model, no types of acoustic emission sensors were used during his experiment. The scalar seismic moments were later calculated from the general formula as:

$$M_0 = \mu D A \tag{2}$$

where μ is the shear modulus, D is the average local seismic displacement and A is the area of the fault. Similar experiment on the same specimen was conducted by McLaskey et al. (2014) and McLaskey & Kilgore (2013) at the USGS, California, with 14 piezoelectric sensors recording the microseismic events during the test. This large model would allow the fault to be studied realistically so that some parts of it could slide while the rest was not slipping. In this way, individual stick-slips can occur during the loading with the possibility that they might trigger other slides. However, since this specimen had been used for 25 years resulting in many stick

slip events and cumulative slips without additional surface preparation, McLaskey et al. (2014) believed that the present surface was smoother than what it was in 1981.

The test setup was a steel frame with four flatjacks between the frame and the specimen as shown in Figure 2. The model was loaded in σ_2 direction and unloaded in σ_1 direction by increasing and decreasing the pressures slowly along the 1 and 2 directions, respectively, with the same rate of 0.001 MPa/s. This way, the normal pressure on the fault was kept constant while the fault was shearing. They tried to model the earthquake cycle by loading, resetting and holding at four stages. Slip sensors were installed on top of the fault to measure relative slips from one side of the fault to the other. Piezoelectric sensors were also installed on top and bottom of the fault. The sensors would respond to the vertical component of motion in frequency ranges of ~100 Hz to ~1 MHz and were installed 200 mm off the fault. The onset of instability was observed at 3.7 MPa of shear stress. At this point, the fault would experience several small falls and rises in the shear stress each accompanied by a small displacement along the fault. These small displacements have been reported to range from 0.08 to 0.15 mm (McLaskey, 2013). The shear modulus and critical slip distance of the Sierra white granite were estimated to be around 20 GPa and 5 micron, respectively (McLaskey, 2013).
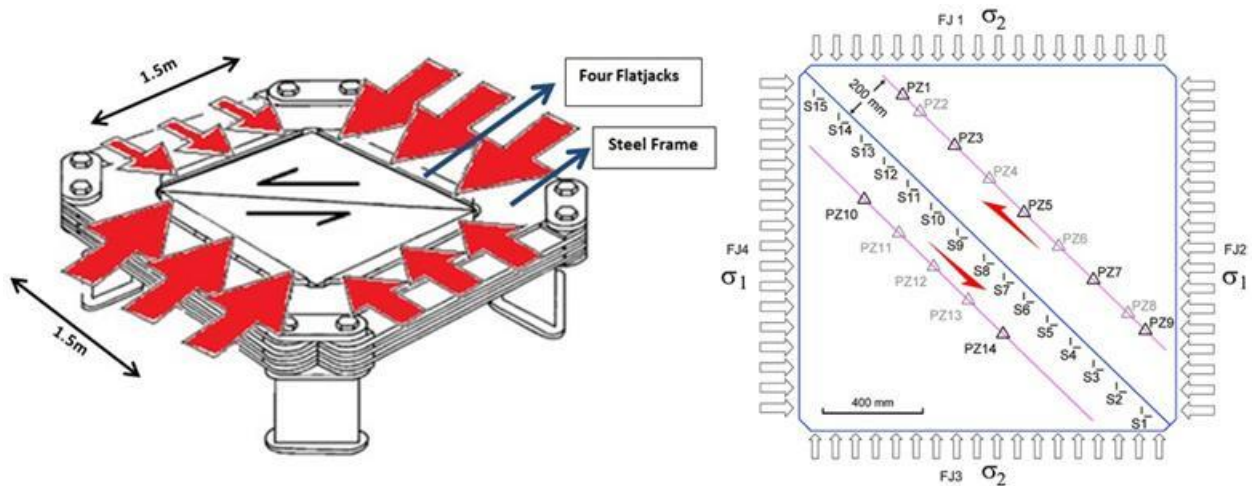
Figure 2: (Left) McLaskey's experimental setup. (Right) Slip sensors and piezoelectric sensors. Piezoelectic sensors are mounted on top and bottom of the sample. Flatjacks are marked with FJ1 to FJ4. Strain gages are shown by S1 to S15. (McLaskey & Kilgore, 2013)

4. Numerical Model

In this research, Particle Flow Code (PFC3D) v.5.0 is used to model the experiment reported by McLaskey & Kilgore (2013). PFC3D is an explicit implementation of Distinct Element Method (DEM) developed by Itasca and despite continuum models does not require mesh generation. In this code, it is assumed that the particles are rigid (non-deformable). In a PFC3D model, particles are bonded by models such as Parallel Bond Model and Smooth Joint Model. Parallel bonds can transmit both forces and moments and can be envisioned as a short length beam or a "set" of elastic springs uniformly distributed over a circular cross section at the contact point (Potyondy & Cundall, 2004).

Smooth joint model is used to simulate interfaces. The traditional way to model an interface is to change the properties such as strength of the bonds along the interface to those representing the real interface. The problem with this approach is bumpiness of the boundaries that can affect the behavior of the system. The effect of these bumpy boundaries could become more

important, when it comes to modeling joints or weak planes. A possible solution is to use smaller size particles along the interface which is not practical in large models. In order to solve this problem, another type of bond that simulates an "interface" regardless of the orientation of the particles along it, is "Smooth Joint Contact Model" (Mas Ivars et al., 2008). This model could be assigned to all the contacts between particles that lie on or along the opposite sides of the interface. This model overcomes the drawback of the boundaries that are bumpy. The reason for calling it "smooth" is because of the constitutive behavior that allows particles bonded by this contact model to overlap and to "slide" on each other instead of moving around one another. Once a smooth joint model is created, the already existing contact or parallel bond models are deleted automatically for the contacts along the interface. Figure 3 shows the behavior of smooth joint model compared to the usual parallel bond model.

In PFC3D, it is assumed that due to small timesteps, a disturbance cannot propagate farther than neighbor particles and therefore velocities and accelerations can be considered constant during each cycle. Once a force is applied to the model, integrating twice the Law of Motion using the timestep, velocities and then displacements are calculated that result in the updated position of each particle. The updated positions are then used by the Force-Displacement Law to calculate the new forces and so on. This process of cycling is continued until a pre-defined criterion is met.
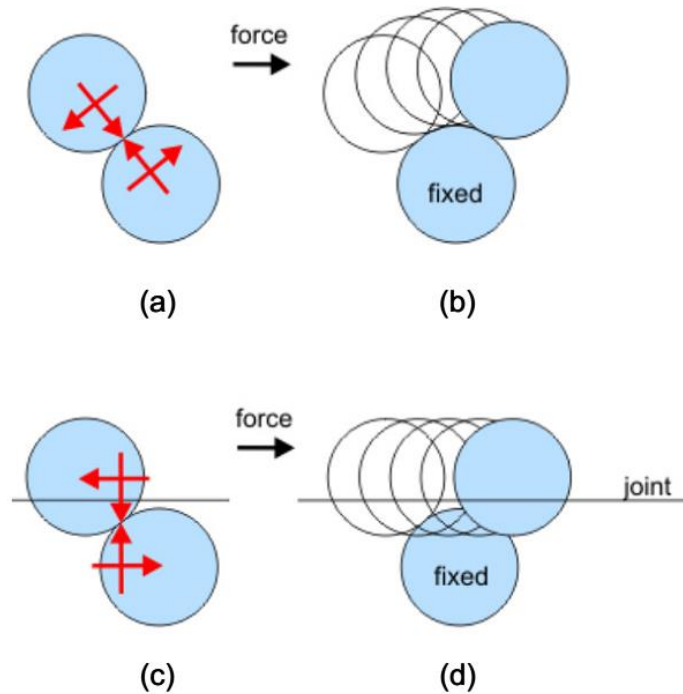
Figure 3: a) standard contact model with relative normal and tangential forces with regard to their orientation b) displacement of the particles bonded by standard contact model assuming the bottom ball is fixed c) normal and tangential forces on the particles whose contact is located along the smooth joint regarding their orientation with respect to the joint c) displacement of particles bonded by smooth joint model (Mas Ivars, 2008)

4.1. Algorithm for Recording Slip-Induced Microseismicity

The numerical representation of the fault is composed of all the contact points whose at least one of the particles is located along the fault. Once a slip occurs at any of these contacts, if the normal stress of that contact is greater than 0.1 MPa, an "event" is created and the time at which slip initiated is recorded. The reason for this threshold can be explained using Figure 1 (left). According to this Figure, if the simple static-dynamic friction law (dotted blue curve) is used instead of the realistic frictional resistance curve (solid red), the rate of decrease in frictional resistance during slip will always be faster than the rate of decrease in driving force and thus every slip will be seismic. It is known that low stiffness, high normal stress and small D_C facilitate the unstable slip (Dieterich, 1979). Based on Eq. (1), assuming the frictional

properties and the stiffness of surroundings are constant along the fault, normal stress will be the only controlling factor for the onset of instability and thus a low normal stress results in the fault sliding stably. Therefore, it is necessary to set a minimum normal stress for the slips to be considered seismic. In practice, this threshold has the advantage of reducing the number of recorded events and faster computation time (Hazzard & Pettitt, 2013). However, it will be shown in section 4.3.2. of this paper that the models presented in this study are not sensitive to this threshold.

According to laboratory stick-slip friction data reported by McGarr (1994), the dynamic friction in this study has been assumed equal to 80% of the static friction. Therefore, once a slip passes the normal stress criterion, the coefficient of friction of that contact is dropped to 80% of its original value. Once the contact stops sliding, the coefficient of friction is readjusted to its static value. This is implemented to take into account the healing phenomenon (due to processes such as creep in the field or thermal mechanism in the lab causing the micro-asperities to weld together) that is believed to be a necessary component for generation of earthquakes in nature (McLaskey et al., 2012). For each seismic slip, the start and end times as well as displacement of the contact are recorded. Considering each slip as one event, results in all the magnitudes to be almost equal. A good practice is to assume a group of slips close in time and space forming a slip patch and clustering them to form a single event. Therefore, the events have been clustered if they had two conditions: they were within a space window and their duration of slip would overlap for at least one cycle. Another criterion has also been implemented for duration of each slip. Assuming the shear can propagate as slowly as 0.5 times the shear wave velocity of the material (Hazzard & Young, 2000), the minimum duration of a slip to be considered seismic is calculated as:

13

$$T_{\min} = \text{int}\left(\frac{space\_window}{0.5 \times ae\_svel}\right) \tag{3}$$

where T_{min} is the time required for the shear wave to propagate the space window, *space_window* is considered to be 0.42 m in this study and *ae_svel* is the shear wave velocity equal to 2700 m/s for Sierra granite as reported by McLaskey et al. (2014). Equation (3) shows that not only the choice of space window affects the size of clusters and therefore distribution of events' magnitudes, but also it affects the minimum lifetime of a slip to be considered seismic.

Therefore, choosing an appropriate space window can be considered as part of the model's calibration. For a similar clustering algorithm but for crack induced events, Hazzard (1998) showed that the space window of 5 particle diameters would yield the best results in a 2D model and above this value, the b-values were not dependent on the size of window while for a 3D model a smaller space window would be more reasonable. Later in a study of unstable fault slip in Lac Du Bonnet granite, Hazzard et al. (2002) showed that 3 particle diameters would result in a realistic b-value. In the present model, considering the maximum diameter of the particles is 0.14 m, a space window equal to 0.42 m (3 particle diameters) has been used. Comparison of the results with data reported by McLaskey et al. (2014) and McLaskey & Kilgore (2013) that will be shown in the next sections confirms this has been an appropriate choice.

At the end of the test, all the slips that occurred within the space window and with the durations overlapping at least 1 cycle are clustered together. The area of each clustered event is calculated assuming the event as an ellipse. The largest and smallest radii of the ellipse are calculated based on the farthest and closest particles to the center of the event, respectively.

In order to calculate the centroid of each event, the number of contacts forming that event has been used. However, it has to be emphasized that the number of "contacts" forming an event is not necessarily the same as the number of "slips" forming that event. As an example, the clustering process for three smooth joint contacts, A, B and C, is schematically illustrated in Figure 4.
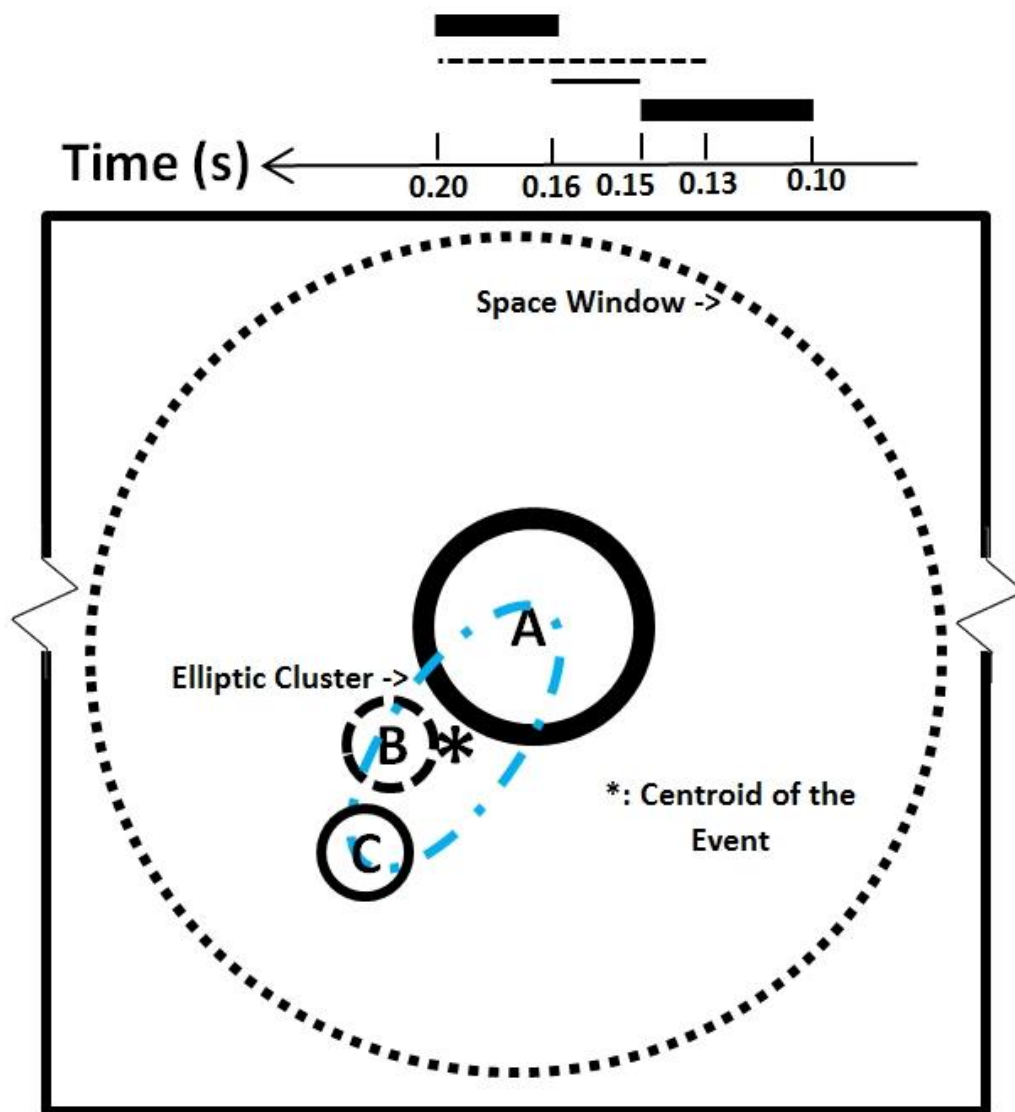

Figure 4: A section of the fault illustrating the clustering process for three contacts, A, B and C. It's assumed no other contacts within the space window slipped from 0.10 to 0.20 s. Size of the elliptic event is determined based on the closest and farthest contacts to the center of the event (i.e. B and A, respectively)

In this Figure, imagine contact A starts slipping from 0.10 s to 0.15 s. At 0.13 s contact B starts slipping within the space window of contact A and therefore; so far these two slips constitute one event. The contact B slips until 0.20. At 0.15 s contact C starts slipping until 0.16 s at which point contact A starts slipping "again" until 0.20 s. No other contacts slipped within the space window of contact A from 0.10 s to 0.20 s. In this example, although there are 4 slips forming one event, there are only three contacts involved and therefore, the location of contact A is used once for calculating the centroid (although it slipped twice). The centroid is simply calculated as the average of the locations of the contacts forming the event. Average displacement is calculated as the sum of all displacements associated to all the slips, 4 slips in this example, forming one event divided by the number of contacts in that event/cluster. Having the area of the event and the average displacement of all the contacts forming the cluster, seismic scalar moment, *Mo,* is calculated using Eq. (2). Eventually, magnitudes are calculated using Eq. (3):

$$M_w = \frac{2}{3}\log M_0 - 6.0 \tag{3}.$$

The whole idea of clustering is justified considering the fact that in nature, most seismic events are made up of small ruptures and shearing of asperities (Scholz, 2002).

4.2. Results

A discrete element model of the experiment reported by McLaskey et al. (2014) and McLaskey & Kilgore (2013) is made by PFC3D as shown in Figure 5. There are six walls surrounding the model. The wall on the face is not shown in this Figure to make the balls visible. The balls are bonded together by parallel bond model. In order to resemble the fault, smooth joint model has

been installed in all the contacts of all the particles located along the diagonal fault extending from top right to the bottom left of the model.
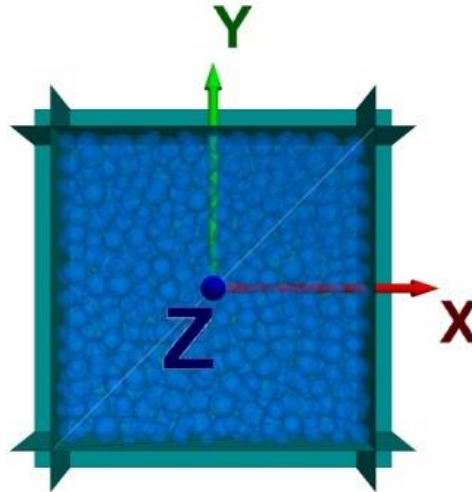

Figure 5: The PFC3D model. The fault extends from the top right to the bottom left

There is no direct one to one correspondence between the micro parameters of a discrete element model and macro parameters of the real rock. Therefore, the calibration process involves some trial and error attempt of varying the micro parameters until the desired macro response is observed (Itasca, 1999). However, in the present model, in order to eliminate the effect of possible bond breakages (cracks) on the fault's behavior, the strength properties of parallel bonds were set to high values so that they would not control the results and therefore, such calibration for the parallel bond properties was no longer necessary. The fault (smooth joint) parameters were chosen so that the expected stick-slip behavior would be observed at the onset of instability at about 3.7 MPa as reported by McLaskey & Kilgore (2013). In order to keep the normal stress on the fault constant at 5 MPa during the test, the top and bottom walls were moving inwards while the right and left walls were moving outwards all four with the same velocity. The two walls on the back and front were not moving during the test. However, it has to be kept in mind

that due to complete symmetry in the fault's location and loading scheme of this test as well as high strength properties of the parallel bonds, there will be practically no damage in any part of the model other than slip along the fault. The PFC3D parameters of the model are summarized in Table 1.

Table 1: Micro-parameters used in PFC3D model of Sierra granite

Ball Parameters		Smooth Joint Parameters		
Average radius (m)	Young's modulus (GPa)	Normal stiffness (N/m^3)	Shear stiffness (N/m^3)	Coefficient of static friction
md_ravg	**ba_Ec**	**sj_kn**	**sj_ks**	**sj_fric**
0.056	2.1E10	2.1E10	2.1E10	1.05

As the first pass to validate the model, the normal stress along the fault has been obtained during the test. In PFC3D, it is possible to record the stress and strain values in three different ways: wall-based, measurement-sphere based and particle-based. The wall based stresses are calculated as the sum of out-of-balance forces of all the particles in contact with the wall divided by the wall's area. Measurement-spheres (or "circles" in 2D) are representative volumes in which an average value for the stress or strain is calculated. They can be defined at arbitrary places in the specimen. Particle based measurements represent the value of stress at one particular point.

In order to ensure the normal stress remains constant on the fault, the wall-based stresses (shown in dashed red and purple in Figure 6) have been monitored. Considering the whole model as one big element, the normal stress on the fault, however, is calculated using a 2D transformation matrix as shown in Eq. (4):

$$\sigma_n^{fault} = \frac{\sigma_x + \sigma_y}{2} - \frac{\sigma_x - \sigma_y}{2} \cos 2\theta - \tau_{xy} \sin 2\theta \qquad (4)$$

18

where θ is 45°, τ_{xy} is assumed to be negligible and σ_x and σ_y are wall-based stresses along the x and y directions, respectively. As another measure of assurance, the normal stress on the fault is also determined by summing up all the normal forces of all the contacts with the smooth joint model assigned to them divided by their area. The wall-based and directly-measured normal stresses along the fault as well as the wall-based stresses along the x and y directions are plotted in Figure 6. As can be observed in this Figure, if the onset of instability is assumed as the point at which the increase in shear stress stops (i.e. 3.7 MPa), this point corresponds to about 0.22 s past the start of the test. Despite the laboratory experiment which has practical limitations for how much the fault can slip, in this PFC3D model, there is really no criterion for when the test should stop. Therefore, the test was stopped once 0.1% total displacement of the fault (i.e. 2 mm) was reached. Total displacement of the fault is calculated mathematically from the wall-based strains in the x and y directions.
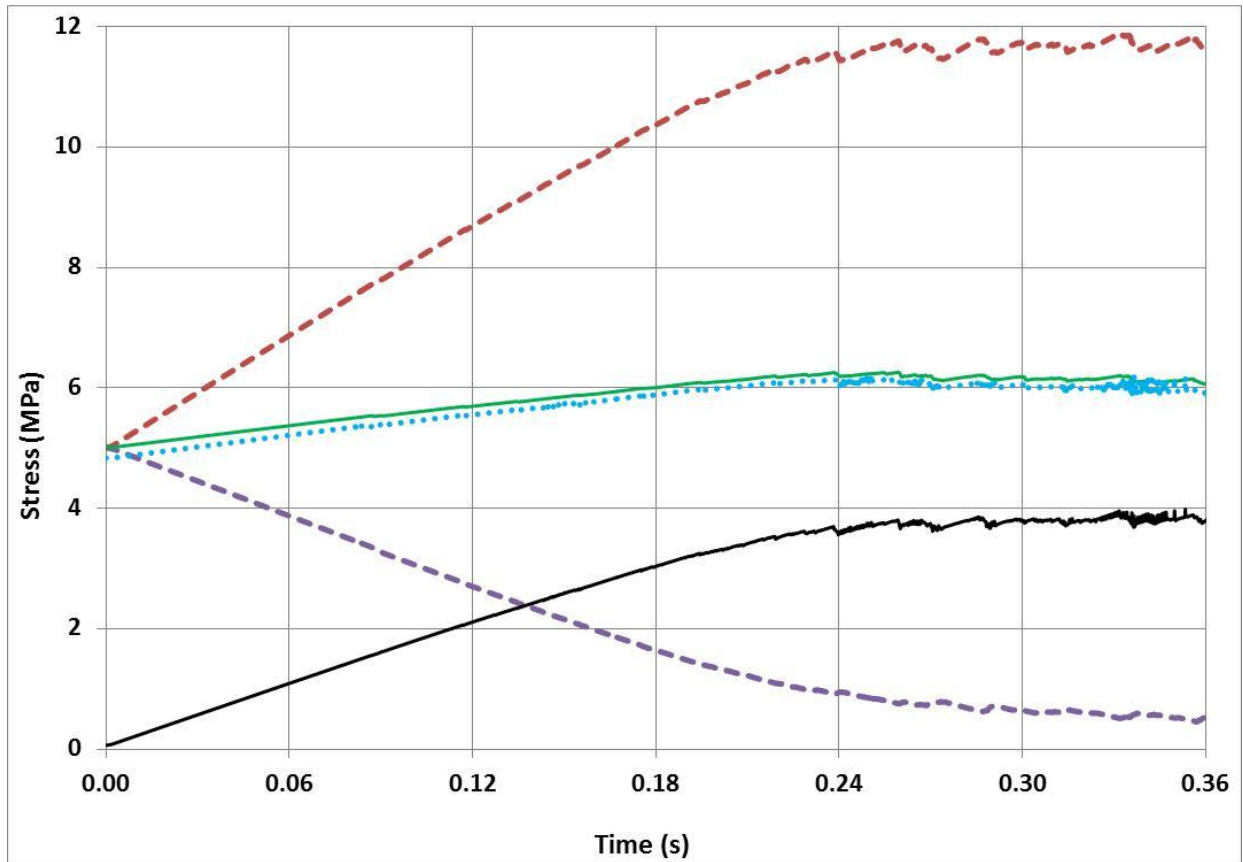
Figure 6: Stress measurements during the test. Dotted blue curve starting at 5 MPa is the direct measurement of normal stress from the particles along the fault. The solid green curve at 5 MPa is the normal stress along the fault determined from the wall based stresses by the transformation matrix. The solid black curve starting at 0 MPa is shear stress along the fault directly measured from the smooth joint contacts. The two dashed symmetrical red and purple curves are the wall-based stresses along the x and y directions, respectively.

As can be observed in Figure 6, the normal stress directly measured from the balls is a little bit smaller than the wall-based measurement which is as expected since the fault is modeled as a discontinuum surface. Other than that, the normal stress along the fault has been kept constant during the test. The overall shear stress along the fault versus time as well as a magnified section of the final stick-slip behavior is plotted in Figure 7.
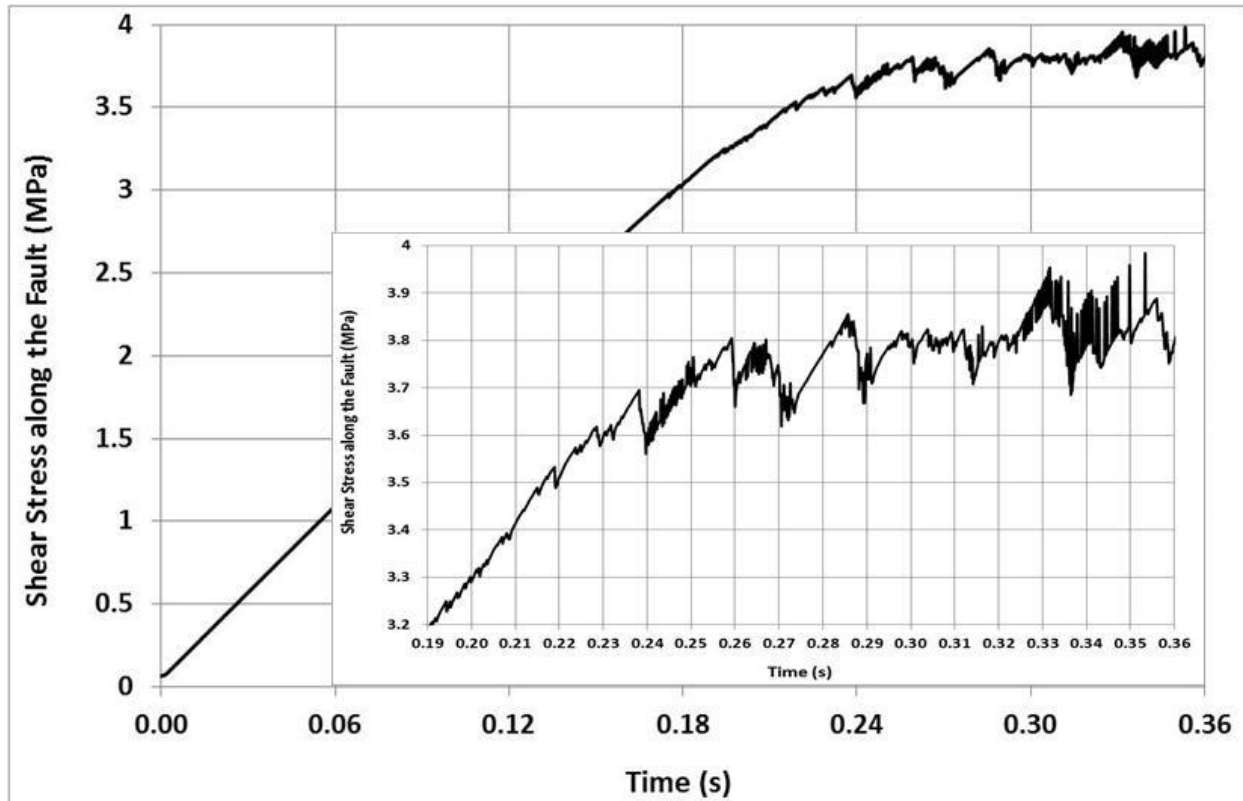
20

Figure 7: The average shear stress along the fault versus time. Shear force is a vector with 3 components. Average shear stress of all the contacts with smooth joint model along the x and y directions are calculated by summing up their respective forces divided by their areas. Then, the average shear stress along the 45º fault has been calculated by the stress transformation matrix.

As can be observed in this Figure, the stick slips have been successfully modeled by the numerical model. Prior to the onset of instability at 3.7 MPa, McLaskey and Kilgore (2013) observed a linearly increasing shear stress throughout the test. An interesting observation from this Figure is that 3 stages in the slip behavior of the fault can be identified. The first stage is from 0 to about 3.2 MPa where the shear increases linearly with no major stick slips. The second stage starts from 3.2 MPa until about 3.7 MPa with minor stick slips while the shear is still increasing but non-linearly (i.e. the strength is still mobilizing). The final stage starts from 3.7 MPa where the falls and rises of shear stress become more significant and the overall trend of shear stress becomes almost constant while the fault is sliding.

Location of the slips at two sides of the fault recorded in the PFC3D model is shown in Figure 8. As can be observed in this Figure, the events are uniformly spread along the fault. This is in agreement with the observation of McLaskey et al. (2014).
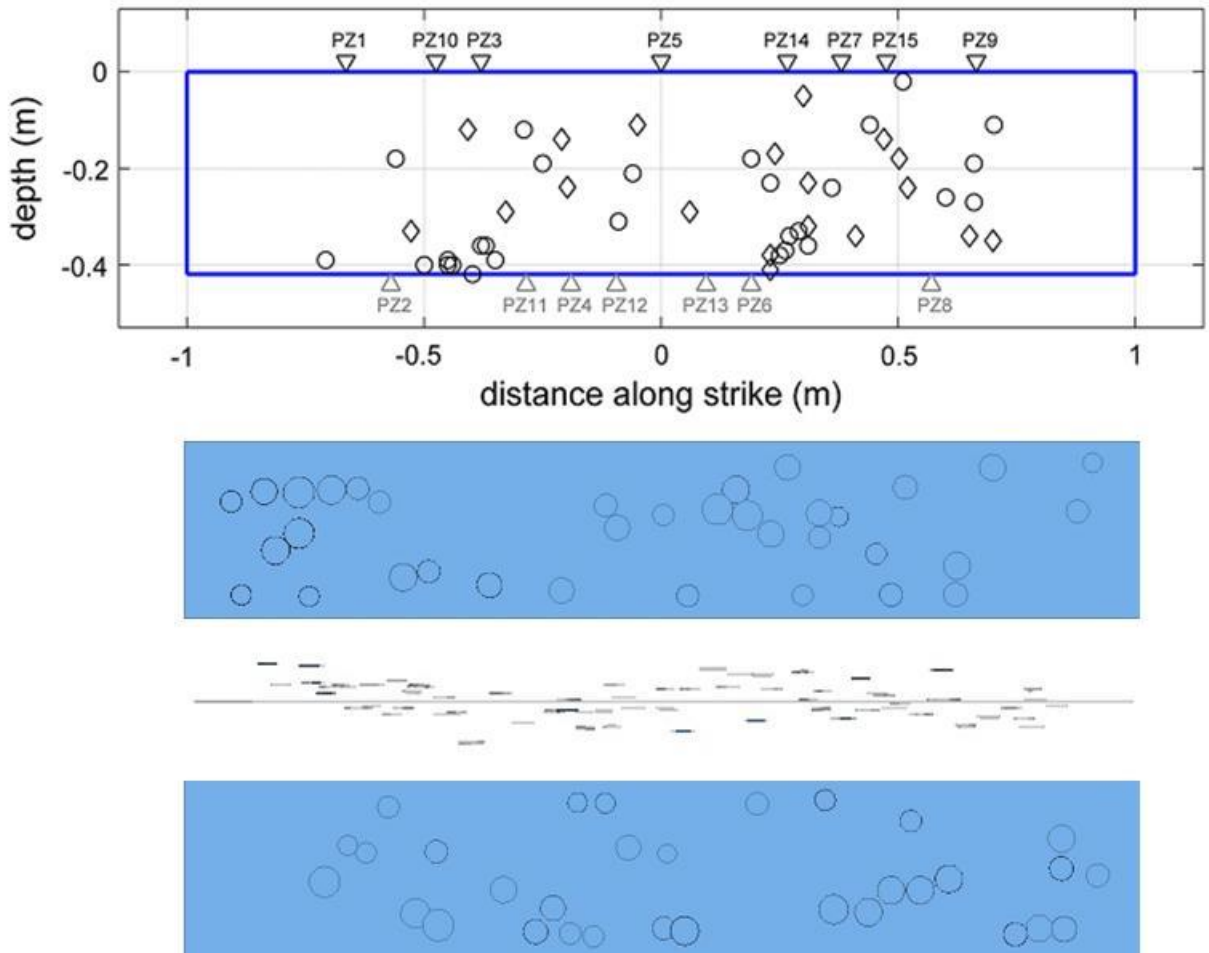

Figure 8: The top figure shows the location of events reported by (McLaskey et al., 2014). Foreshocks and aftershocks are shown by circles and diamonds, respectively. They have not reported the events near the fault ends. The two figures at the bottom with blue background are the location of slips in the PFC3D model at both sides of the faults. The figure between these two is a side view of the fault with the location of events around it. No clustering is shown in this figure.

In the PFC3D model, 223 slips have been recorded with the majority of magnitudes around -6 and some -7. As was previously mentioned, a reasonable approach would be to cluster the slips close in time and space to represent more realistic events. After clustering, the number of events

is reduced to 131. As can be observed from the clusters shown in Figure 9, the largest events have occurred at the central section of the fault which is in agreement with McLaskey & Kilgore (2013). Due to difficulties in plotting ellipses, all the events in Figure 9 are illustrated with circles with diameters equal to the major axis of ellipses; otherwise as mentioned before, the area of each event has been calculated assuming it has an elliptic shape in general. It has to be emphasized that the number of events in a PFC model is a function of model's resolution and therefore it is not reasonable to compare the number of PFC events directly with the real number of events recorded in the experiment.
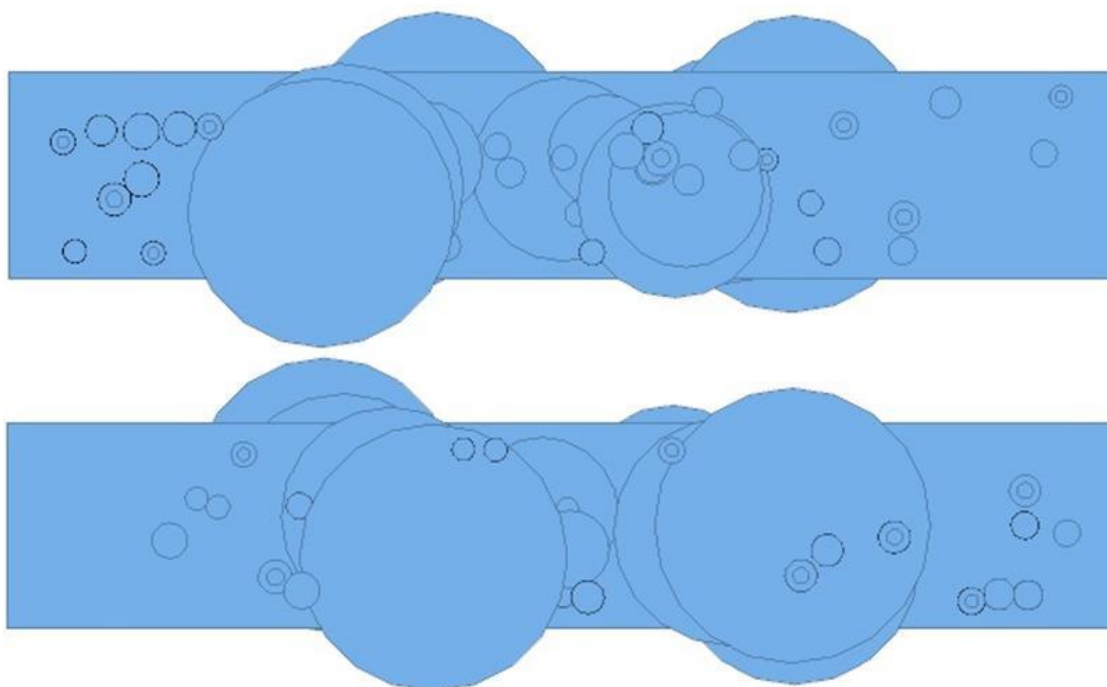

Figure 9: The clustered events in PFC3D model. A bigger radius shows a larger patch. Concentric circles represent consecutive slips on the same contact.

In their experiment reported in 2013 (McLaskey & Kilgore, 2013) the normal stress along the fault was kept constant at 5 MPa. However, in their recent 2014 publication, the test has been repeated with 4 and 6 MPa normal stresses along the fault. McLaskey et al. (2014) were able to

accurately locate 16 and 32 events for the test with 4 and 5 MPa normal stresses, respectively. In order to determine the mechanism of events, they performed a moment tensor inversion technique and reported that the majority of the events could be modeled by double couple mechanism resulted from frictional slips. The average displacement of each dynamic slip event (DSE) was reported to be about 50-150 microns occurring in about 3-5 ms with the source radii about 3-6 mm. A few larger foreshocks (M>-5.0) were not reported due to difficulty in analyzing them. In the PFC3D model, there are 98 smooth joint contacts forming the fault. The stick-slip behavior of a group of them during the test is shown in Figure 10.

Although a general trend of increase in the shear stress followed by stick slips is observed for the fault in Figure 7, it can be observed from Figure 10 that different contacts do not necessarily follow the same stick slip pattern. In other words, for the small patches along the fault, not every drop in shear stress corresponds to a drop in the normal stress. This suggests the likelihood of existing of another process responsible for generation of local stick-slips. It is in agreement with McLaskey & Kilgore (2013) that some aseismic slips can possibly trigger repeated earthquakes in their vicinity.
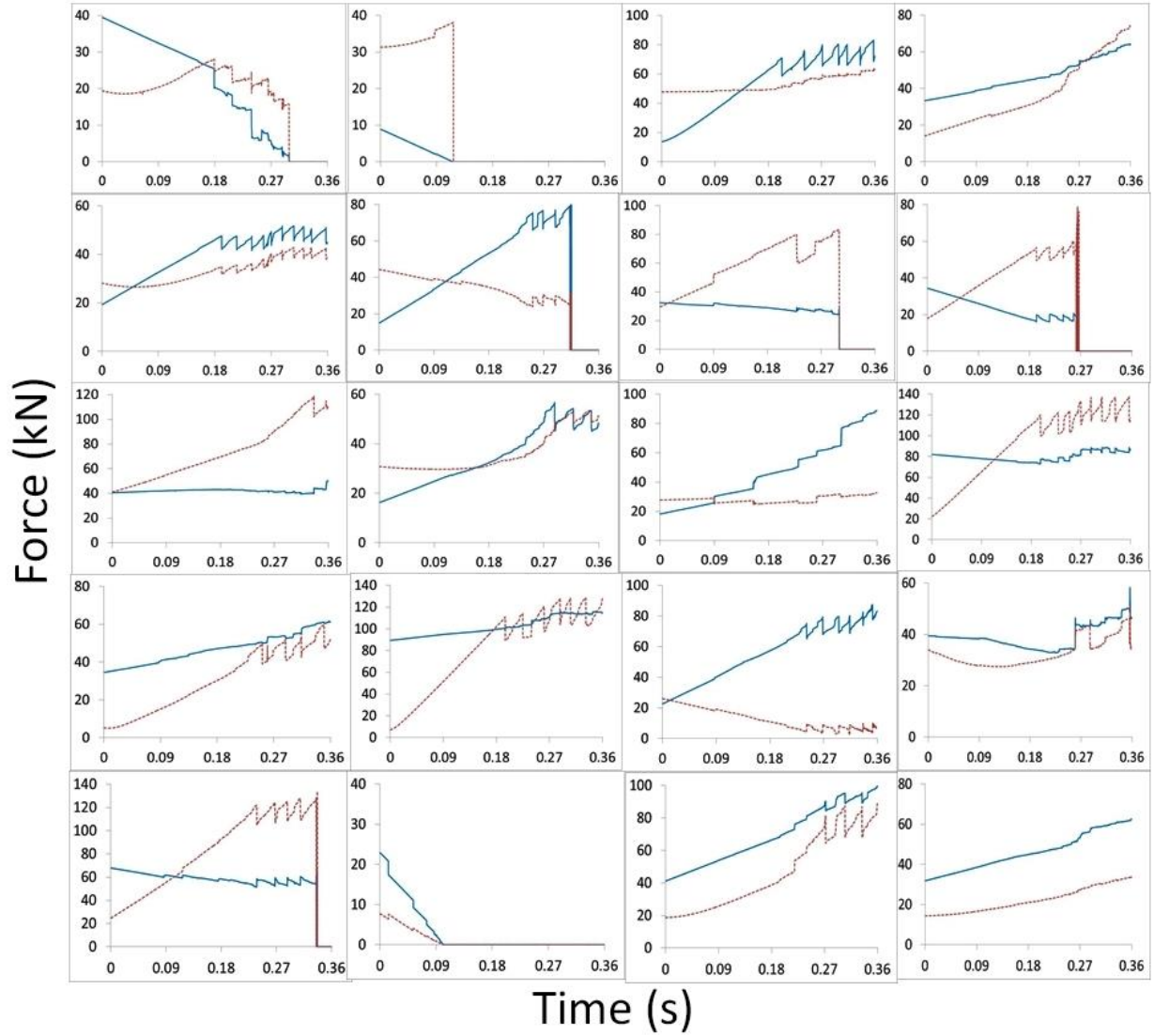
Figure 10: Variations of stick-slip behavior in different contacts along the fault. Normal and shear forces are shown with solid blue and dashed red, respectively.

4.3. Parametric Study

A parametric study is presented in this section to investigate the effect of various parameters on the shear behavior of the fault as well as on generation of microseismic events.

4.3.1. Studying the Effect of Space Window's Size

A model with the same properties as mentioned in Table 1 is repeated with different space window's sizes of 0.14, 0.28 and 0.42 m (equal to 1, 2 and 3 times the maximum diameter size of the balls, 0.14 m). In order to calculate the magnitudes, the shear modulus of 2 MPa has been used for the slipping patch in all the tests. The b-value plots as well as variations in the number of events for the three tests are shown in Figure 11.
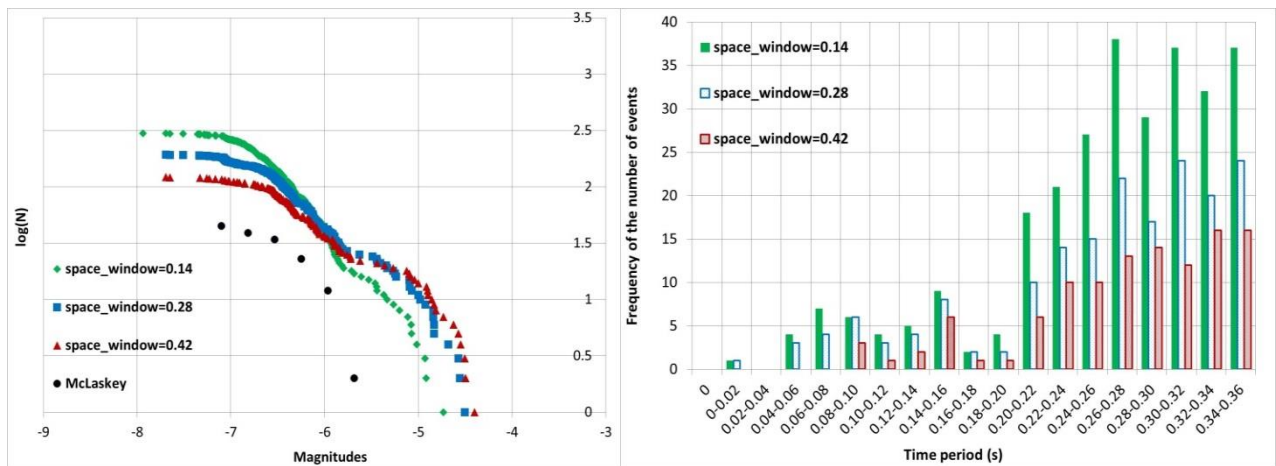

Figure 11: b-value plots as well as frequency of the number of events recorded during the tests for three different sizes of space windows

As can be observed in this Figure, an increase in the size of space window causes an increase in the appearance of magnitudes larger than -6 while for the smaller magnitudes, a reverse effect is observed. A comparison between the numerical b-value plots with the experiment is not accurate due to three reasons: a) McLaskey's data belong to the tests with 4 and 6 MPa normal stress (not 5 MPa) b) The loading in this study was continuous while in order to simulate the earthquake cycle their experiments would include loading, resetting and holding at four stages and c) Some magnitudes greater than -5 have not been reported by them. However, for the sake of comparison and considering the b-values, regardless of a-values, the size of space window

equal to 3 times the maximum diameter of the balls, 0.42 m, seems to provide the best match with reality and therefore, it has been used for the other tests presented in the paper.

Also, a fewer number of clusters have been observed for greater sizes of space window which is as expected.

4.3.2. Studying the Effect of Normal Stress Threshold for Seismic Events

A model with the same properties as mentioned in Table 1 is repeated with three normal stress thresholds of 0.0 MPa (i.e. no threshold), 0.1 MPa and 3 MPa for the slips to be considered seismic (Figure 12). As was mentioned in section 4.1., although for the slips that pass the normal stress threshold the coefficient of friction is decreased to 80% of the static friction and thus it would affect the shear strength as well, no significant difference in shear-displacement and displacement-time plots was observed and therefore they are not included in the paper. However, as was expected, a lower threshold would result in a greater number of smaller events and also earlier appearance of events in the shear process. The b-values do not seem sensitive to this threshold.

In nature, the overall normal stress on the fault would depend on the in-situ stresses as well as orientation of the fault while for the local patches along the fault, heterogeneity would also play a role. Therefore, this threshold would be more important if faults with different resolutions and or faults in different stress regimes were being compared. However, for the conditions tested in this section, the behavior of model does not seem sensitive to the choice of this threshold and thus 0.1 MPa has been used for the other tests presented in next sections.
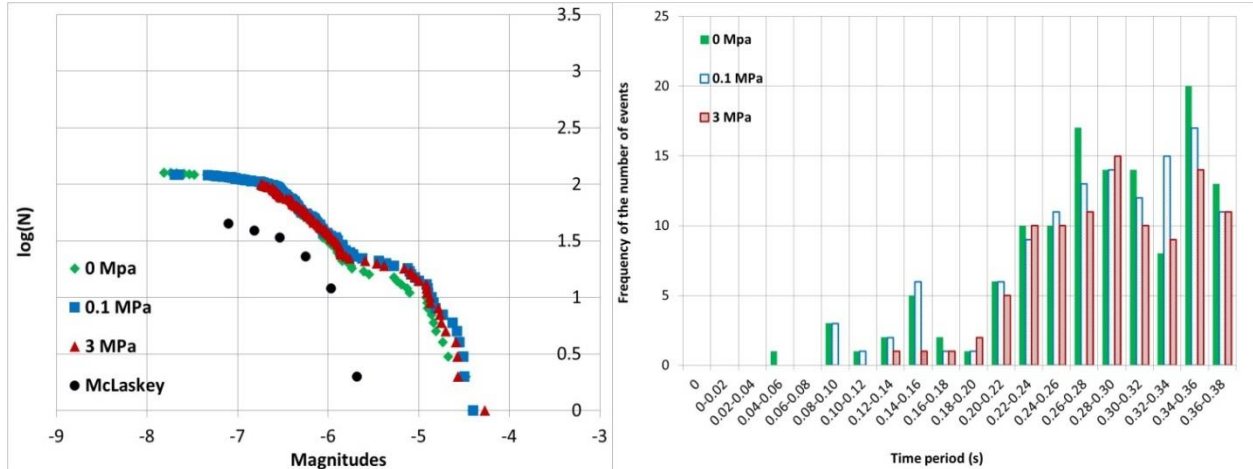
27

Figure 12: Variations of model's behavior for different normal stress thresholds for the slips to be considered seismic

4.3.3. Studying the Effect of Discretization (Size of Particles)

A model with the same properties as listed in Table 1 has been repeated with finer and coarser particles. The average radii of the particles in the three tests were 0.081 m (199 balls), 0056 m (649 balls) and 0.029 m (5164 balls). As shown in Figure 12, coarser balls would result in higher strengths, greater stress drops during stick-slip, slower rate of displacements and smaller b-values. Although the events appear earlier in the finer model and the number of events are higher, the second stage in transitioning from elastic linear increase in shear strength to the final instability where the shear stress becomes constant, from 85% to peak strength, is less obvious in the finer model. This could be observed both in the shear-displacement plots and in frequency of events versus time plots where the slope of getting to the peak number of events is very steep for the finest model (Figure 13).
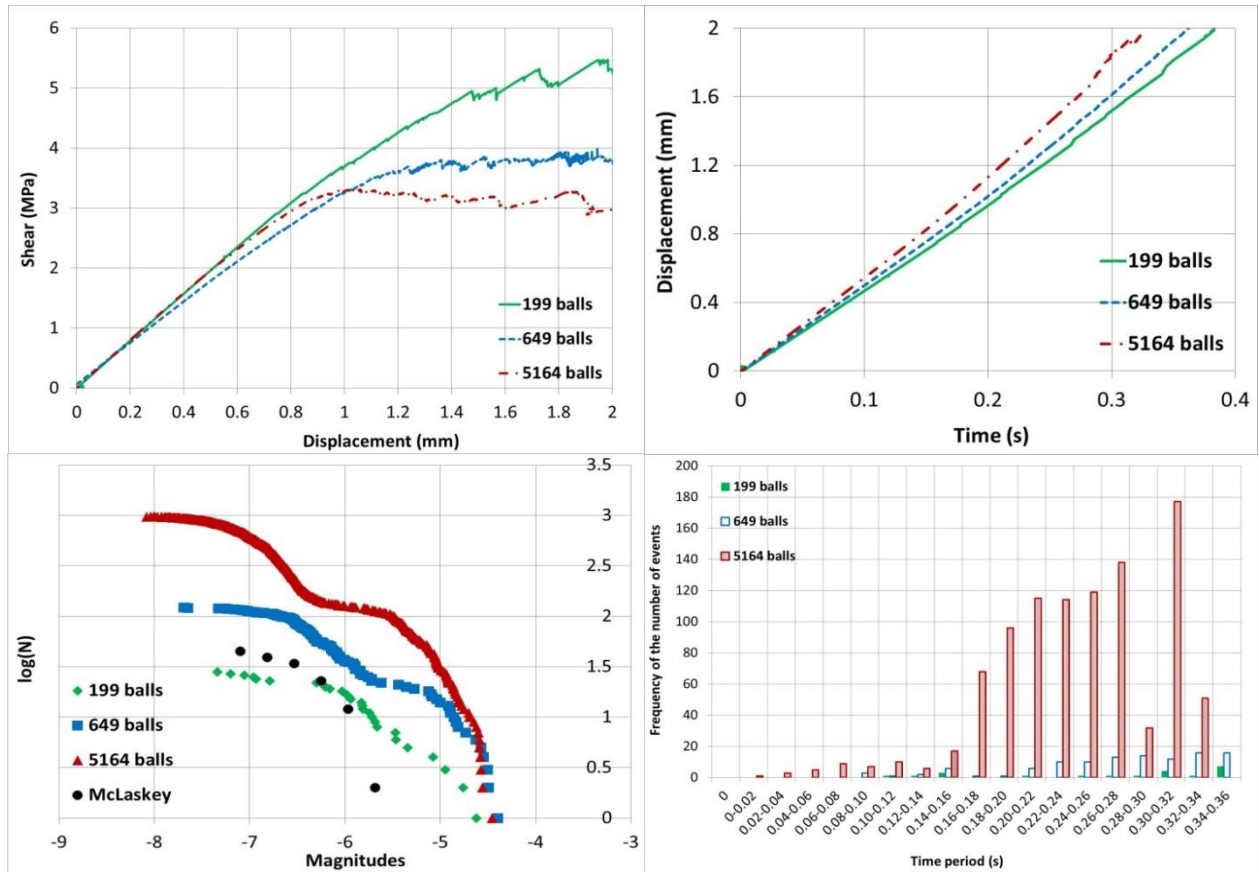
Figure 13: Variations of model's behavior for different resolutions

4.3.4. Studying the Effect of Fault's Coefficient of Friction (sj_fric)

A model with the same properties as mentioned in Table 1 is repeated with different fault's coefficient of friction (1.05, 0.85 and 0.55) which is within the range from 0.6 to 1 as suggested by (Byerlee, 1978). The results shown in Figure 14 indicate a decrease in overall shear strength as well as an increase in the rate of displacements for smaller coefficients of friction. The number of magnitudes larger than -5.5 are not much sensitive to the fault's coefficient of friction while an increase in the frequency of events smaller than -5.5 is observed for smaller coefficients which is consistent with the greater number of events observed for these faults.
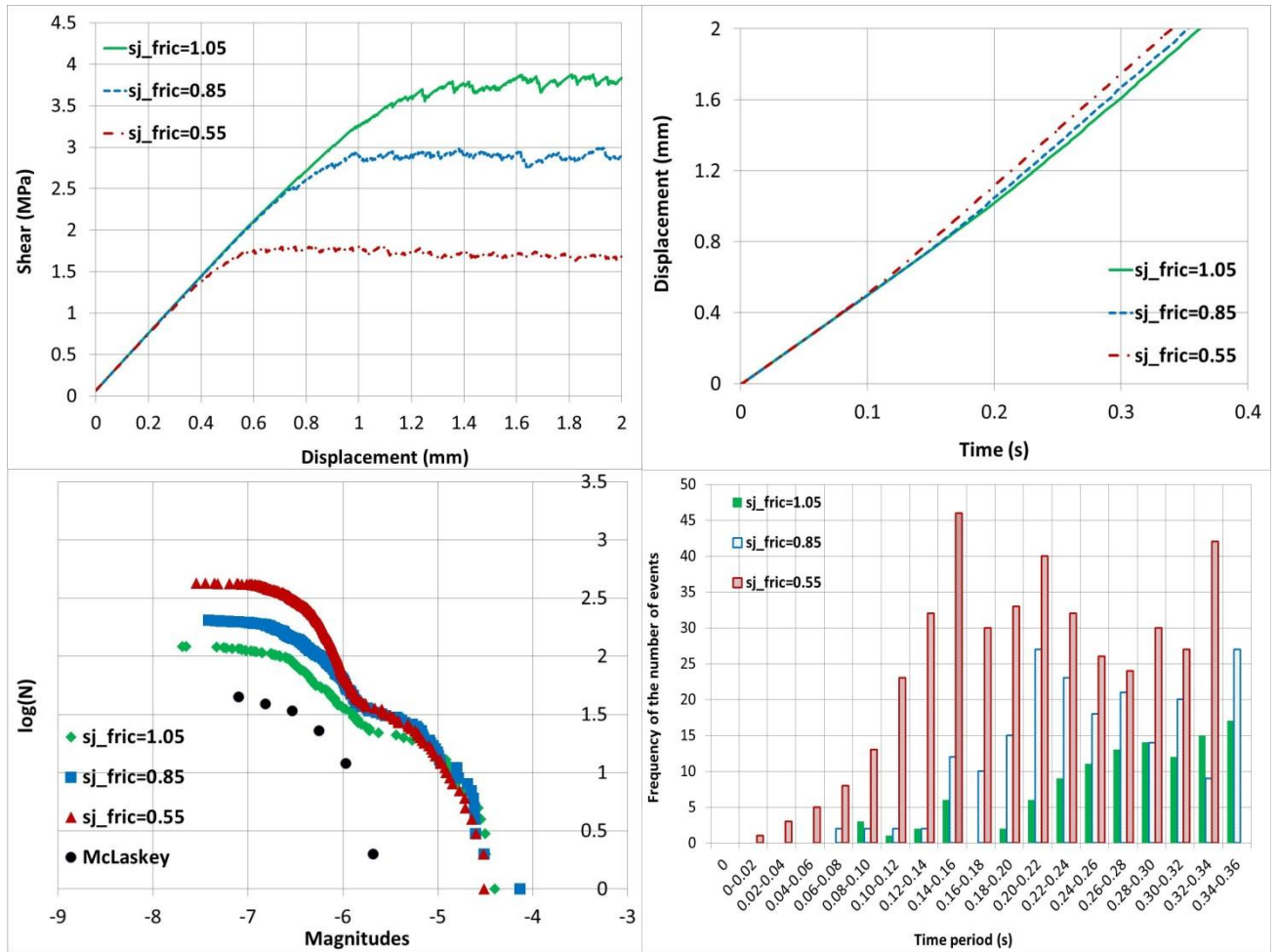
Figure 14: Variations of model's behavior for different coefficients of friction

4.3.5. Studying the Effect of Particles Elasticity (ba_Ec)

A model with the same properties as mentioned in Table 1 is repeated with varying the Young's modulus of the balls (2.1e9, 2.1e10 and 2.1e11). This would represent the stiffness of the medium surrounding the fault. As shown in Figure 15, for the softest model (ba_Ec=2.1e9), small stick-slip instability was observed as early as 0.1 mm displacements were reached. This behavior continued until about 7 mm displacements (at 3.7 MPa shear stress) that could be considered as the onset of the second stage. The peak shear strength, 4.4 MPa, was reached after

9.6 mm displacements and 1.9 s after the start of the test. This is much longer compared to previous cases where the maximum shear strength was reached in a fraction of a second. The overall pattern of shear-displacement for the fault with softest surrounding (i.e. ba_Ec=2.1e9) included three stages in shear process similar to the model with Young's modulus of balls equal to 2.1e10, but only the portion until 2 mm displacement is shown in Figure 15.

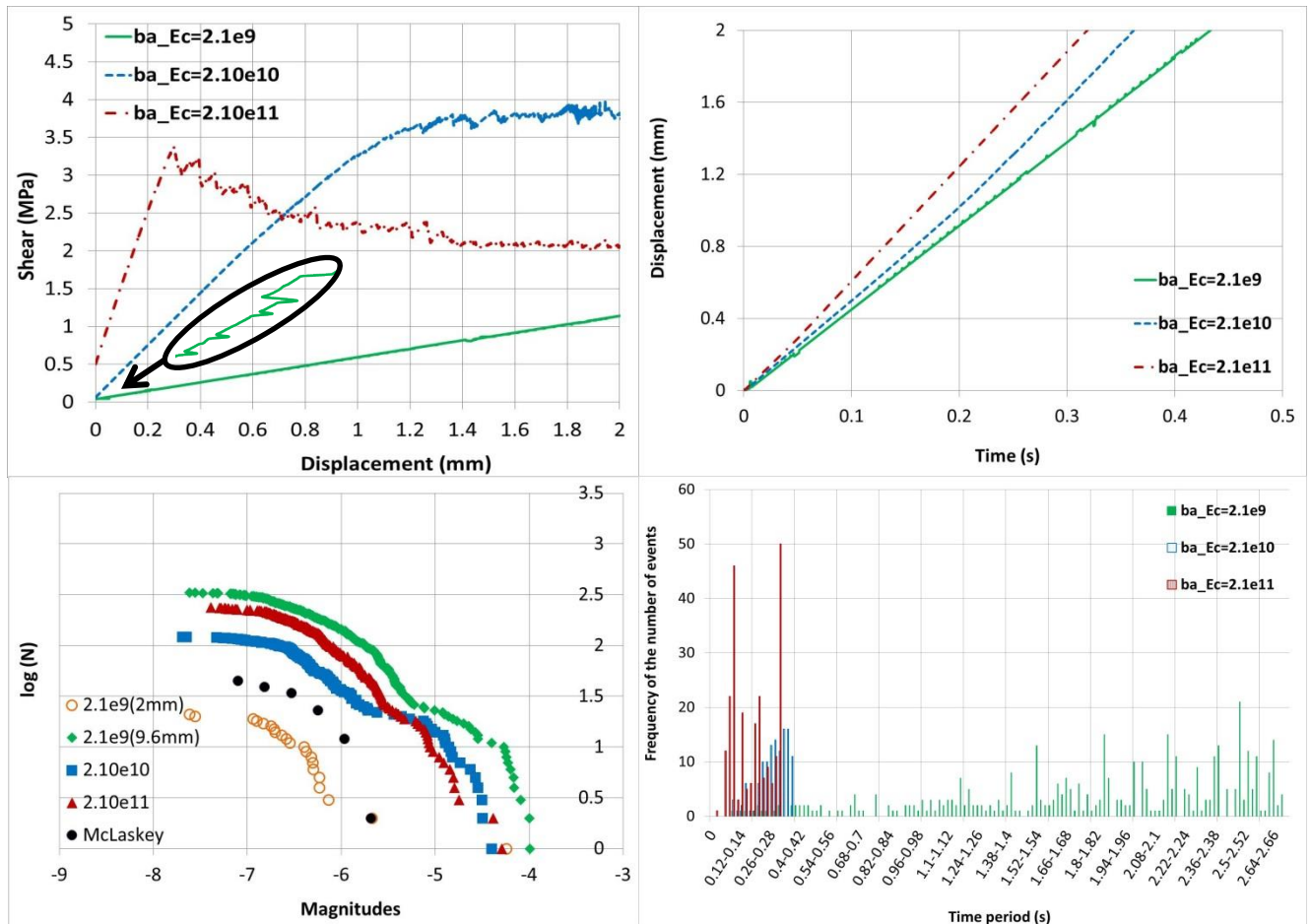**Figure 15: Variations of model's behavior for different Young's modulus of the particles. Distribution of magnitudes for the softest model are plotted based on the events recorded until 2 mm and 9.6 mm displacements**

For the model with the surrounding harder than the fault itself a softening behavior is observed with almost no second stage in the shear process. With regard to the number of events, a softer

surrounding has not resulted in more emissions for the same amount of displacement and its only contribution has been to delay the process of displacements. An overall shift in the a-values towards larger magnitudes is also observed for the faults with softer surrounding while the b-values are not much sensitive.

4.3.6. Studying the Effect of Fault's Elasticity (sj_kn & sj_ks)

A model with the same properties as mentioned in Table 1 is repeated with varying the elastic properties of the smooth joint. As shown in Figure 16, higher shear strengths are observed for harder faults. The rate of deformations and b-value plots, however, do not seem to be much affected. A lower number of events is observed for softer faults.
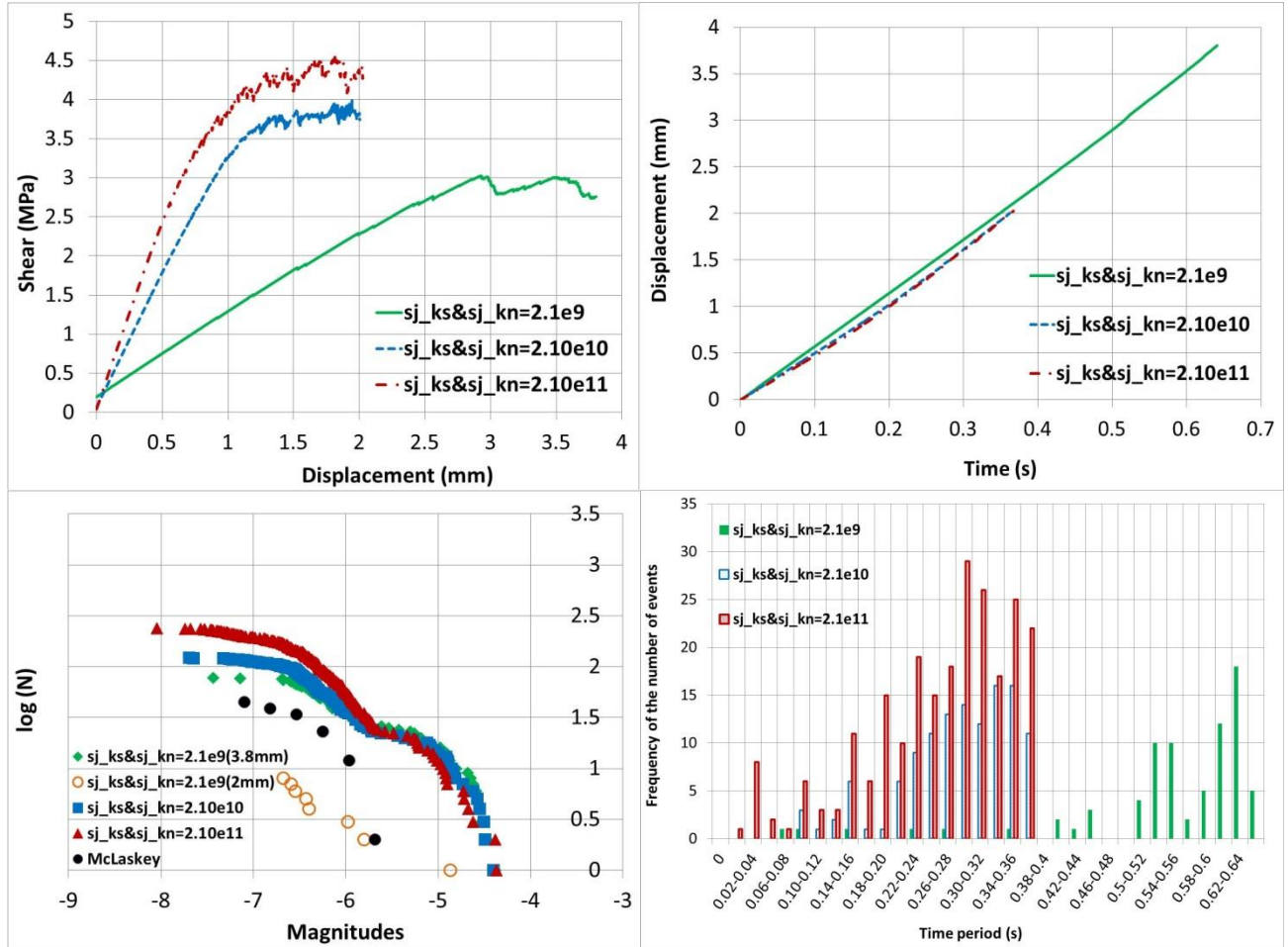
Figure 16: Variations of model's behavior for different elastic properties of the fault. Distribution of magnitudes for the model with softest fault properties are plotted based on the events recorded until 2 mm and 3.8 mm displacements

4.3.7. Studying the Effect of Normal Stress

A model with the same properties as mentioned in Table 1 is repeated with normal stresses along the fault equal to 3, 5 and 7 MPa. The plots in Figure 17 show an increase in the shear strength as well as a decrease in the rate of deformations for higher normal stresses. Also, for the same amount of deformation, higher normal stresses generate fewer emissions. An overall decrease in the b-value can be observed for higher normal stresses as well.
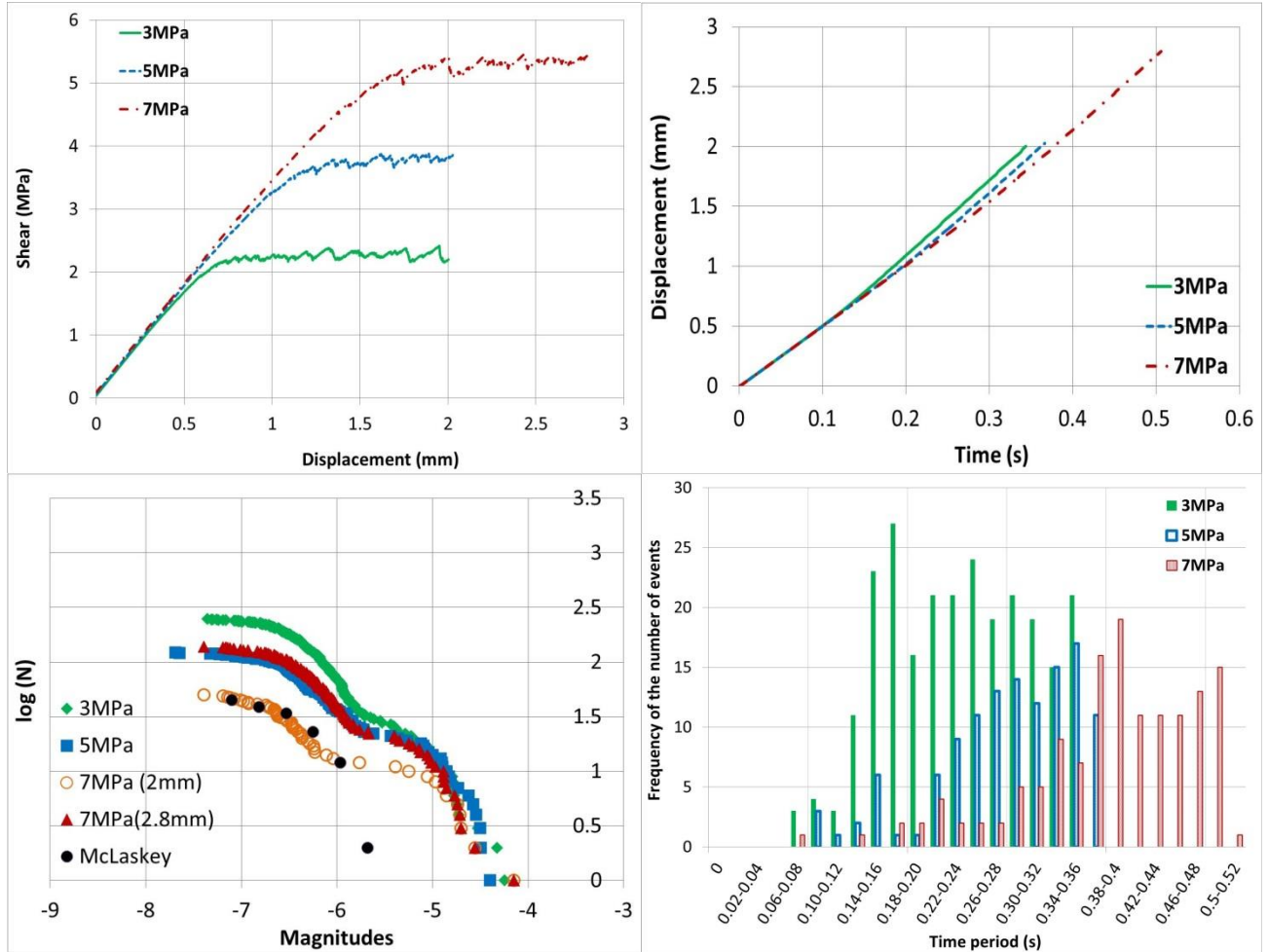
Figure 17: Variations of model's behavior for different normal stresses. Distribution of magnitudes for the model with 7 MPa normal stress are plotted based on the events recorded until 2 mm and 2.8 mm displacements

5. Discussion

As was expected before, the behavior of the numerical model was sensitive to the elastic properties of the medium surrounding the fault as well as fault's properties and the size of particles. It is in agreement with the fundamental mechanism shown in Figure 1. Sensitivity of the numerical model to the frictional parameters is also in agreement with the observation of McLaskey et al. (2014) who believed the recorded events were not due to factors such as grain crushing or fracturing of the fresh rock. The majority of events were believed to have a double-

34

couple mechanism indicating a shear dislocation along the fault. The ones with non-double-couple mechanism were expected not to exceed 20% of all the events (McLaskey et al., 2014).

They observed no specific difference between the focal mechanisms and magnitudes or even stress drop of the foreshocks and aftershocks. Both types of events were broadly distributed along the fault. This is consistent with the results of numerical modeling presented in this study. The results show that largest magnitudes appear mostly in the last stage of unstable stick-slip once the peak shear strength of the fault is already reached.

According to the model shown in Figure 1 (left), whether or not a slip is seismic (or aseismic) would depend on the elasticity of the medium (i.e. stiffness of spring in this model) as well as the amount of stress drop due to unloading the normal stress or frictional properties of the surface. In Figure 15, it was shown that stick-slips would occur much earlier in the shear process for the fault with softer surrounding. This is in agreement with the fact that low stiffness facilitates unstable slips (Dieterich, 1979). Also, it has been suggested that local stick-slips could trigger or facilitate other slips in their vicinity (McLaskey & Kilgore, 2013). A possible mechanism for this could be the fact that local slips (or in other words, local unloading normal stress conditions) provide a softened surrounding for their neighbor patches and thus, similar to what was shown in Figure 15, facilitating their instability. The amount of how much either of seismic or aseismic slips would contribute to this could be the subject of another study.

6. Conclusion

Applicability of the discrete element modeling to successfully reproduce stick-slips in large scale that takes a long time and effort in laboratory to be studied was shown in this paper. Once the

model is calibrated with one set of experiment, it can be used to expand our knowledge to the cases that cannot be easily tested.

In this research, the microseismic release along pre-existing faults during shearing was studied numerically. For this purpose, the experiment reported by McLaskey & Kilgore (2013) was modeled using PFC3D. PFC inherently allows modeling of stick-slips however an algorithm is also developed in this research to record the slip-induced acoustic emissions. Some advantages of the present model are: 1) The three dimensional and discrete nature of model that allows taking into account the geometrical heterogeneity and make the simulations more realistic 2) Focusing on the fault's behavior by use of smooth joint model that allows eliminating the bond breakages affecting the results. 3) The algorithm developed for recording the stick-slip induced microseismic events.

Once the results compared well with real laboratory data, the model was then expended upon to study the difference in shear and microseismic behavior in faults with different properties. A summary of the results is presented here:

1- A decrease in shear strength was observed for the models with smaller particles, smaller coefficient of friction of the fault, harder surrounding of the fault (higher Young's modulus for the particles), softer faults (smaller elasticity moduli of the fault) and smaller normal stress on the fault. Also, a softer behavior (i.e. decrease in the initial slope of shear-displacement curve) was observed for the softer faults as well as faults with softer surrounding.

2- A higher rate of displacements was observed for the faults with finer particles, smaller coefficient of friction, harder surrounding and smaller normal stress. The fault's elastic properties

36

did not seem to have much effect on the rate of displacements, however, a small increase in this rate was observed for the softest fault. A comparison between displacement-time and shear-displacement curves suggests that higher rate of displacements are observed for weaker conditions (i.e. conditions resulting in smaller peak strength) while this conclusion seems less obvious for the softer faults (Figure 16).

3- With regard to the magnitudes, a greater size of space window resulted in an increase in the events larger than -6 while a reverse effect was observed for the smaller events. The b-values were not sensitive to the normal stress threshold of slips to be seismic. Increasing the resolution or decreasing the normal stress on the fault both caused an increase in the b-values. Decreasing the coefficient of friction did not have much effect on the magnitudes larger than -5.5 while for the smaller magnitudes, a decrease in this coefficient caused an increase in the number of events. Increasing the particles' elasticity caused a decrease in the a-values but the b-values were not much affected. The b-values were not sensitive to the elastic properties of the fault.

4- A larger number of recorded events were observed for the models with smaller size of space window, smaller normal stress threshold, finer particles, smaller fault's coefficient of friction, harder fault's surrounding, harder fault and smaller normal stress on the fault. An obvious observation is that for the same amount of slip, the emissivity would depend on several factors affecting the release of microseismic energy. It was also suggested that there are three stages in the slip behavior of a fault: 1) linear increase in the shear stress until 85% of the peak strength with no or very few stick-slips 2) stable slip from 85% of the peak shear strength until the maximum shear strength is reached 3) unstable continuation of slip until for some reason the fault stops. An exception was observed for the case with fault's surrounding being harder than

the fault itself (Figure 15) where right after the first elastic stage in the shear process, the third stage started with a post-peak softening pattern. However, among these three stages, the last one which is unstable has the greatest number of stick-slips and therefore, a comparison between the number of events versus time and shear versus displacement plots suggests that for the same amount of displacement, the conditions at which the third stage is reached earlier would be the most emissive ones.

Although due to the geometry of the fault and loading scheme used in this research it was not investigated, the results suggest that in reality it is quite possible for the two ends of a fault to be still while there are patches along the fault undergoing stick-slips. Also, local stick-slips seem to provide a softer surrounding for their neighbor patches favoring their subsequent stick-slips.

With regard to the calibration of model for stick-slip behavior, the onset of instability (peak shear strength) as well as b-value seems to be the two most controlling parameters that need to be taken into account.

Acknowledgement

References

Brace, W. F., & Byerlee, J. (1966). Stick-slip as a mechanism for earthquakes. *Science*, *153*(3739), 990–992.

Brace, W. F., & Byerlee, J. (1970). California earthquakes: why only shallow focus? *Science (New York, N.Y.)*, *168*(3939), 1573–5. doi:10.1126/science.168.3939.1573

Brune, J. N., Brown, S., & Johnson, P. A. (1993). Rupture mechanism and interface separation in foam rubber models of earthquakes: a possible solution to the heat flow paradox and the paradox of large overthrusts. *Tectonophysics*, *218*(1-3), 59–67. doi:10.1016/0040-1951(93)90259-M

Byerlee, J. (1978). Friction of rocks. *Pure and Applied Geophysics PAGEOPH*, *116*(4-5), 615–626. doi:10.1007/BF00876528

Byerlee, J., & Brace, W. F. (1968). Stick slip, stable sliding, and earthquakes—effect of rock type, pressure, strain rate, and stiffness. *Journal of Geophysical Research*, *73*(18), 6031–6037.

Dalguer, L. A., & Day, S. M. (2006). Comparison of fault representation methods in finite difference simulations of dynamic rupture. *Bulletin of the Seismological Society of America*, *96*(5), 1764–1778.

Damjanac, B., Gil, I., Pierce, M., Sanchez, M., Van As, A., & McLennan, J. (2010). A New Approach to Hydraulic Fracturing Modeling In Naturally Fractured Reservoirs. *44th U.S. Rock Mechanics Symposium and 5th U.S.-Canada Rock Mechanics Symposium*. Retrieved from https://www.onepetro.org/conference-paper/ARMA-10-400

Day, S. M., Dalguer, L. A., Lapusta, N., & Liu, Y. (2005). Comparison of finite difference and boundary integral solutions to three- dimensional spontaneous rupture. *Journal of Geophysical Research: Solid Earth (1978–2012)*, *110*(B12).

Dieterich, J. H. (1979). Modeling of rock friction: 1. Experimental results and constitutive equations. *Journal of Geophysical Research*, *84*(B5), 2161. doi:10.1029/JB084iB05p02161

Dieterich, J. H. (1981). Potential for geophysical experiments in large scale tests. *Geophysical Research Letters*, *8*(7), 653–656. doi:10.1029/GL008i007p00653

Fairhurst, C. (2013). Fractures and Fracturing:
Hydraulic Fracturing in Jointed Rock. *ISRM International Conference for Effective and Sustainable Hydraulic Fracturing*. Retrieved from https://www.onepetro.org/conference-paper/ISRM-ICHF-2013-012

Finch, E., Hardy, S., & Gawthorpe, R. (2003). Discrete element modelling of contractional fault-propagation folding above rigid basement fault blocks. *Journal of Structural Geology*, *25*(4), 515–528. doi:10.1016/S0191-8141(02)00053-6

Galis, M., Moczo, P., & Kristek, J. (2008). A 3-D hybrid finite-difference—finite-element viscoelastic modelling of seismic wave motion. *Geophysical Journal International*, *175*(1), 153–184.

Hazzard, J. (1998). *Numerical modelling of acoustic emissions and dynamic rock behaviour. [electronic resource]*. University of Keele.

Hazzard, J., Collins, D. S., Pettitt, W. S., & Young, R. P. (2002). Simulation of unstable fault slip in granite using a bonded-particle model. In *The Mechanism of Induced Seismicity* (pp. 221–245). Springer.

Hazzard, J., & Pettitt, W. S. (2013). Advances in Numerical Modeling of Microseismicity. In *47th US Rock Mechanics/Geomechanics Symposium*. American Rock Mechanics Association.

Hazzard, J., & Young, R. P. (2000). Simulating acoustic emissions in bonded-particle models of rock. *International Journal of Rock Mechanics and Mining Sciences*, *37*(5), 867–872. Retrieved from http://cat.inist.fr/?aModele=afficheN&cpsidt=1419981

Hazzard, J., & Young, R. P. (2002). Moment tensors and micromechanical models. *Tectonophysics*, *356*(1), 181–197.

Hazzard, J., & Young, R. P. (2004). Dynamic modelling of induced seismicity. *International Journal of Rock Mechanics and Mining Sciences*, *41*(8), 1365–1376.

Itasca, C. G. (1999). PFC 3D-User manual. *Itasca Consulting Group, Minneapolis*.

Jansen, F. (2006). Numerical Simulation of Stick-slip Processes with Application to Seismology and Rock Glacier Dynamics.

Julian, B. R., Miller, A. D., & Foulger, G. R. (1998). Non-double-couple earthquakes 1. Theory. *Reviews of Geophysics*, *36*(4), 525. doi:10.1029/98RG00716

Kristiansen, T. G., Barkved, O., & Pattillo, P. D. (2000). Use of passive seismic monitoring in well and casing design in the compacting and subsiding Valhall field, North Sea. In *EUROPEC: European petroleum conference* (pp. 231–241).

Mas Ivars, D. (2008). Bonded-Particle Model for the Deformation, Yield and Failure of Jointed Rock Masses. In *PhD Thesis*. Stockholm, Sweden.

Mas Ivars, D., Potyondy, D. O., Pierce, M., & Cundall, P. A. (2008). The smooth-joint contact model. *Proceedings of WCCM8-ECCOMAS*.

McGarr, A. (1994). Some comparisons between mining-induced and laboratory earthquakes. *Pure and Applied Geophysics PAGEOPH*, *142*(3-4), 467–489. doi:10.1007/BF00876051

McLaskey, G. C. (2013). Personal communication.

McLaskey, G. C., & Kilgore, B. D. (2013). Foreshocks during the nucleation of stick-slip instability. *Journal of Geophysical Research: Solid Earth*, *118*(6), 2982–2997. doi:10.1002/jgrb.50232

McLaskey, G. C., Kilgore, B. D., Lockner, D. A., & Beeler, N. M. (2014). Laboratory Generated M -6 Earthquakes. *Pure and Applied Geophysics*. doi:10.1007/s00024-013-0772-9

McLaskey, G. C., Thomas, A. M., Glaser, S. D., & Nadeau, R. M. (2012). Fault healing promotes high-frequency earthquakes in laboratory experiments and on natural faults. *Nature*, *491*(7422), 101–104. Retrieved from http://dx.doi.org/10.1038/nature11512

Mora, P., & Place, D. (1994). Simulation of the frictional stick-slip instability. *Pure and Applied Geophysics*, *143*(1-3), 61–87.

Morgan, J. K. (2004). Particle Dynamics Simulations of Rate- and State-dependent Frictional Sliding of Granular Fault Gouge. *Pure and Applied Geophysics*, *161*(9-10). doi:10.1007/s00024-004-2537-y

Nielsen, S., Carlson, J. M., & Olsen, K. B. (2000). Influence of friction and fault geometry on earthquake rupture. *Journal of Geophysical Research*, *105*(B3), 6069. doi:10.1029/1999JB900350

Nielsen, S., Knopoff, L., & Tarantola, A. (1995). Model of earthquake recurrence: role of elastic wave radiation, relaxation of friction, and inhomogeneity. *Journal of Geophysical Research: Solid Earth (1978–2012)*, *100*(B7), 12423–12430.

Ohnaka, M. (1973). Experimental studies of stick-slip and their application to the earthquake source mechanism. *Journal of Physics of the Earth*, *21*(3), 285–303.

Peng, Z., & Gomberg, J. (2010). An integrated perspective of the continuum between earthquakes and slow-slip phenomena. *Nature Geoscience*, *3*(9), 599–607. doi:10.1038/ngeo940

Persson, B. N. J., & Tosatti, E. (1999). Theory of friction: elastic coherence length and earthquake dynamics. *Solid State Communications*, *109*(12), 739–744.

Place, D., Lombard, F., Mora, P., & Abe, S. (2002). Simulation of the micro-physics of rocks using LSMearth. In *Earthquake Processes: Physical Modelling, Numerical Simulation and Data Analysis Part I* (pp. 1911–1932). Springer.

Potyondy, D. O., & Cundall, P. A. (2004). A bonded-particle model for rock. *International Journal of Rock Mechanics and Mining Sciences*, *41*(8), 1329–1364. doi:10.1016/j.ijrmms.2004.09.011

Rabinowicz, E. (1951). The Nature of the Static and Kinetic Coefficients of Friction. *Journal of Applied Physics*, *22*(11), 1373. doi:10.1063/1.1699869

Rabinowicz, E. (1958). The Intrinsic Variables affecting the Stick-Slip Process. *Proceedings of the Physical Society*, *71*(4), 668–675. doi:10.1088/0370-1328/71/4/316

Roux, P.-F., Marsan, D., Métaxian, J.-P., O'Brien, G., & Moreau, L. (2008). Microseismic activity within a serac zone in an alpine glacier (Glacier d'Argentiere, Mont Blanc, France). *Journal of Glaciology*, *54*(184), 157–168. doi:10.3189/002214308784409053

Scholz, C. H. (2002). *The mechanics of earthquakes and faulting*. Cambridge university press.

Xing, H. L., Mora, P., & Makinouchi, A. (2004). Finite element analysis of fault bend influence on stick-slip instability along an intra-plate fault. In *Computational Earthquake Science Part I* (pp. 2091–2102). Springer.

Young, R. P., Collins, D. S., Hazzard, J., Pettitt, W., & Baker, C. (2001). *Use of acoustic emission and velocity methods for validation of micromechanical models at the URL*. Toronto, Ont.: Ontario Power Generation, Nuclear Waste Management Division.

Young, R. P. … Dedecker, F. (2005). Seismic Validation of 3-D Thermo-Mechanical Models for the Prediction of the Rock Damage around Radioactive Waste Packages in Geological Repositories-SAFETI. *Final Report, European Commission Nuclear Science and Technology*.

Zhao, X., & Young, R. P. (2011). Numerical modeling of seismicity induced by fluid injection in naturally fractured reservoirs. *Geophysics*, *76*(6), WC167–WC180.